J Biol Phys (2008) 34:577–590
DOI 10.1007/s10867-008-9122-z

ORIGINAL PAPER

Hydration Profiles of Amyloidogenic Molecular Structures

Florin Despa · Ariel Fernández · L. Ridgway Scott · R. Stephen Berry

Received: 25 June 2008 / Accepted: 20 October 2008 /
Published online: 15 November 2008

Abstract Hydration shells of normal proteins display regions of highly structured water as well as patches of less structured bulk-like water. Recent studies suggest that isomers with larger surface densities of patches of bulk-like water have an increased propensity to aggregate. These aggregates are toxic to the cellular environment. Hence, the early detection of these toxic deposits is of paramount medical importance. We show that various morphological states of association of such isomers can be differentiated from the normal protein background based on the characteristic partition between bulk, caged, and surface hydration water and the magnetic resonance (MR) signals of this water. We derive simple mathematical equations relating the compartmentalization of water to the local hydration fraction and the packing density of the newly formed molecular assemblies. Then, we employ these equations to predict the MR response of water constrained by protein aggregation. Our results indicate that single units and compact aggregates that contain no water between constituents induce a shift of the MR signal from normal protein background to values in the hyperintensity domain (bright spots), corresponding to bulk water. In

F. Despa (✉)
Department of Pharmacology, University of California, Davis, CA 95616, USA
e-mail: fdespa@ucdavis.edu

A. Fernández
Department of Bioengineering, Rice University, Houston, TX 77251, USA

L. R. Scott
Department of Computer Science, The University of Chicago, Chicago, IL 60637, USA

L. R. Scott
Department of Mathematics, The University of Chicago, Chicago, IL 60637, USA

L. R. Scott
Institute for Biophysical Dynamics, The University of Chicago,
Chicago, IL 60637, USA

R. S. Berry
Department of Chemistry, The University of Chicago, Chicago, IL 60637, USA

contrast, large plaques that cage significant amounts of water between constituents are likely to generate MR responses in the hypointensity domain (dark spots), typical for strongly correlated water. The implication of these results is that amyloids can display both dark and bright spots when compared to the normal gray background tissue on MR images. In addition, our findings predict that the bright spots are more likely to correspond to amyloids in their early stage of development. The results help explain the MR contrast patterns of amyloids and suggest a new approach for identifying unusual protein aggregation related to disease.

Keywords Protein hydration · Protein aggregation · Amyloids · Alzheimer's disease · Conformational diseases · Biological water · Magnetic resonance imaging

1 Introduction

Dynamics of water in cells and biological tissues is coupled to the local macromolecular environment [1–14]. Therefore, structural alterations of cellular proteins change the distribution and dynamics of surrounding water molecules. Recent studies [9, 12] suggest that proteins bearing pathological defects, i.e., proteins exhibiting poorly dehydrated backbone H bonds (dehydrons) [15–18], are characterized by an average energy of hydration which is significantly below that corresponding to native proteins. The entropy of water next to these structural defects is unexpectedly large and much shorter than at the other surface sites [9]. The dual behavior of the solvation water described by De Simone et al. [9], i.e., water with regions of highly structured water molecules as well as delineated patches where the local water is less structured and has an increased mobility, is quite similar to that observed in protein unfolding [19, 20]. In these studies [19, 20], magnetic relaxation dispersion curves of protein solutions revealed a significant increase of the short-lived water proton populations next to proteins undergoing unfolding due to physical stresses. Studying the behavior of the hydration water around such protein surfaces is crucial for understanding folding stability and aggregation and may help to design new capabilities of amyloid detection. Here, we provide a mathematical framework for correlating various morphological states of a system of test proteins undergoing aggregation with the characteristic water distribution profiles in the local environment. The present approach can constitute a basis for developing experimental protocols that exploit changes in dispersion properties of surrounding water to assess noninvasively the early stage of amyloidogenic toxic accumulations in cells and tissues.

The basic questions to be addressed are as follows. Let us assume a microscopic environment V containing N proteins, each protein having an intrinsic volume V_m, in a V_w content of water ($V \cong NV_m + V_w$). Suppose we add ΔN test isomers in this environment (Fig. 1). The surfaces of these test isomers have increased densities of patches around which water molecules are less structured (have a bulk-like behavior). As control, we consider a similar-sized environment in which all $N + \Delta N$ constituents are the same. The water content V_w is compartmentalized with respect to the protein structures in four distinct fractions, i.e., bulk, caged, and two categories of surface hydration water (structured and bulk-like). Each compartment (X_j) includes water molecules that have relatively comparable dynamics characterized by an individual mean relaxation time τ_j. Having the characteristic distribution of waters evaluated for the environment in which all $N + \Delta N$ proteins are alike, what is the expected change of the water distribution when the newly

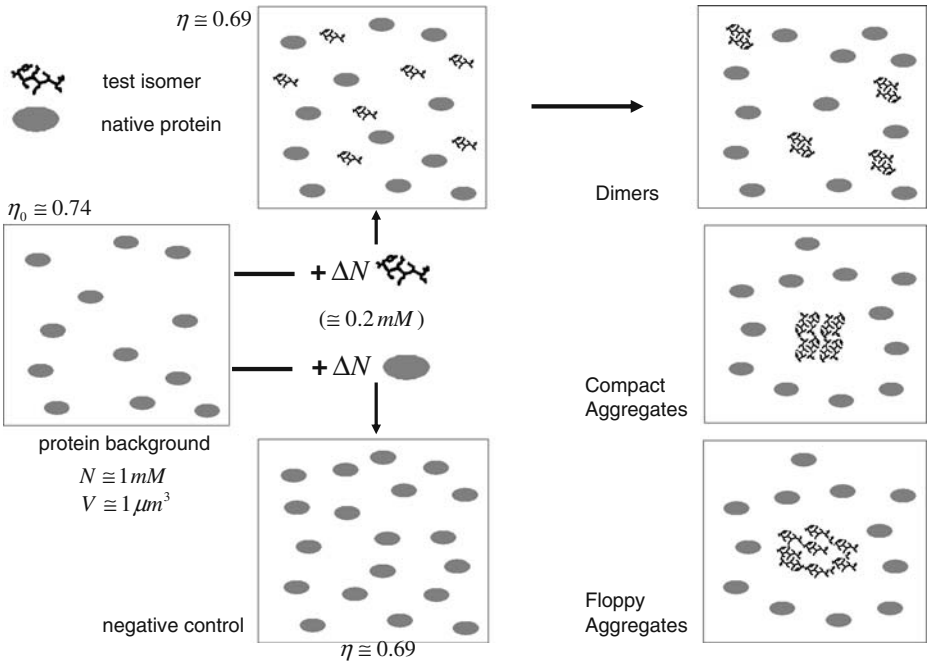

Fig. 1 Insertion of $\Delta N = 0.2\ mM$ test isomers with increased surface densities of patches occupied by bulk-like water ($f^{(A)} > f$) to the protein background ($N = 1\ mM$). As control, we consider a similar-sized environment in which all $N + \Delta N$ constituents are the same, i.e., $f^{(A)} = f$

added ΔN proteins are test isomers, which have distinct surface hydrations? How does this water distribution evolve with increasing the surface density of patches of bulk-like water on the surfaces of these isomers? And what is the relative change of the hydration profile following the morphological transition of the protein system from soluble entities to various molecular composites?

2 Methods

To answer these questions in an effective manner, we construct a mathematical model that describes the compartmentalization of the surrounding water following the addition of ΔN test isomers in the local environment and the association of these isomers in different composites of given structures. We derive simple mathematical equations relating the compartmentalization of water to the local hydration fraction and the packing density of the newly formed molecular assemblies. Then, we employ these equations to predict the magnetic relaxation response of water constrained by protein aggregation.

Test isomers are differentiated from background protein by the fraction of water molecules with a bulk-like behavior (f). f is related to the size of the protein surface area bearing structural defects, which can be estimated from molecular simulations [9, 12, 15–18]. Normally, association of proteins in soluble oligomers squeezes patches of bulk-like waters from the interacting surfaces. These soluble oligomers will eventually aggregate into larger composites, burying all structural defects inside the newly formed macromolecular

assemblies. Long-range interaction between oligomeric composites can also lead to the formation of stable molecular assemblies, caging water molecules inside. The quantity of water sequestered inside the aggregate structure is in direct proportion with the volume of water bound initially to the surface of individual proteins and depends on the average packing density of the aggregate. We are interested to differentiate based on hydration profiles and characteristic magnetic resonance (MR) signals between small compact composites, which are formed by expelling water between constituent units, and loose aggregates, which cage water inside the structure.

2.1 Partition of Water in the Protein System

We write the water fraction η in the form

$$\eta = \frac{V_w}{(N + \Delta N)\, V_m + V_w}, \tag{1}$$

and partition the volume of water (V_w) surrounding the proteins as $V_w = N\,(V_s + V_c) + \Delta N\left(V_s^{(A)} + V_c^{(A)}\right) + V_r$. V_c accounts for water caged in internal cavities and deep peripheral pockets of the protein structure (conserved water), while V_s is the usual amount of water confined at the protein surface. $V_c^{(A)}$ and $V_s^{(A)}$ have similar meanings for the test isomers. In the following, the superscript (A) refers to parameters characterizing test isomers. V_r denotes the remaining hydration water that has a bulk behavior.

2.2 Caged Water

The existence of caged water is reflected in the packing density of the protein, ρ, which is usually defined as $\rho = \frac{V_{vW}}{V_m}$ [21], where V_m is the intrinsic molecular volume of the protein and V_{vW} is the sum of the van der Waals volumes of the constituent atoms of the protein. We can express the amount of caged water as $V_c = V_m - V_{vW} = V_m\,(\rho_{max} - \rho)$, where $\rho_{max} = 0.74$ is the maximum value of random packing [22] considered in the present work. Typically, the value of ρ for a folded protein is about 0.7 [23]. In the following, we assume that this quantity is the same for the test isomers, $V_c \cong V_c^{(A)}$.

2.3 Surface Water

Existing experimental data [4, 19, 20, 24] and theoretical studies [1, 5, 9] show that typical surfaces exhibit sites where water molecules have much higher mobility than at polar surface sites. Let f be the fraction of surface area occupied by these sites and $V_{np} \cong fV_s$ be the amount of water adjacent, or very close, to these sites. The amount of water next to the sites of highly structured water will be $V_p \cong (1 - f)\, V_s$. According to the assumptions of the present model, we can write similar equations for test isomers, $V_{np}^{(A)} \cong f^{(A)} V_s$ and $V_p^{(A)} \cong \left(1 - f^{(A)}\right) V_s$, respectively. The amount of bulk-like water on the surface of the test isomers is assumed to be larger than for the background proteins, as $f^{(A)} > f$.

Based on the scaled particle theory [25], we can express V_s in terms of the molecular volume of the protein, V_m. According to this theory, the intrinsic volume (V_m) of a macromolecule plus a shell of thickness l which results from the mutual thermal motions of the macromolecule and neighboring water molecules form the partial volume V^0, $V^0 \cong V_m + \text{asa}\, l$, where asa represents the water-accessible surface area. V^0 is roughly 1.11 V_m [21] so that the thickness of the hydration shell can be approximated by $l \cong$

$0.11\frac{V_m}{\text{asa}}$ and the volume of water at the macromolecular surface becomes $V_s \cong 0.11 V_m$. We now rewrite the total volume of water surrounding the $N+\Delta N$ soluble peptides in the form

$$V_w = (N+\Delta N)(\rho_{\max}-\rho) V_m + 0.11 V_m \left[(1-f) N + \left(1-f^{(A)}\right)\Delta N\right] + 0.11 V_m \left(fN + f^{(A)}\Delta N\right) + V_r. \tag{2}$$

The right side of Eq. 2 includes the amounts of caged water, highly constrained surface water, less constrained surface (bulk-like) water, and remaining bulk water, respectively. By replacing $V_w = (N+\Delta N) V_m \frac{\eta}{1-\eta}$ from Eq. 1, we obtain

$$1 = \frac{(\rho_{\max}-\rho)(1-\eta)}{\eta} + 0.11 \frac{N(1-f)+\Delta N\left(1-f^{(A)}\right)}{N+\Delta N}\frac{1-\eta}{\eta} + 0.11 \frac{Nf+\Delta N f^{(A)}}{N+\Delta N}\frac{(1-\eta)}{\eta} + X_r, \tag{3}$$

where $X_r = \frac{V_r}{V_w}$. From Eq. 3, we separate and rewrite, for simplicity,

$$\begin{aligned} X_c &= \frac{(\rho_{\max}-\rho)(1-\eta)}{\eta} \\ X_p &= 0.11 \frac{1-\eta}{\eta}\left(1 - \frac{fN + f^{(A)}\Delta N}{N+\Delta N}\right) \\ X_{np} &= 0.11 \frac{1-\eta}{\eta}\frac{Nf+\Delta N f^{(A)}}{N+\Delta N} \\ X_r &= 1 - X_c - X_p - X_{np}, \end{aligned} \tag{4}$$

where X_c is the fraction of caged water; X_p stands for the fraction of highly constrained surface water; X_{np} represents the fraction of less structured surface water and X_r represents the remaining hydration water with a bulk-water behavior. The above Eq. 4 represents a general mathematical description of the compartmentalization of water in a system containing normal proteins and test isomers. They express the water populations X_j, $j = c$, p, np, r, in terms of the local hydration fraction (η), protein numbers (N, ΔN), relative packing density ($\rho_{max} - \rho$), and fractions of surface patches of bulk-like waters (f, $f^{(A)}$).

2.4 Recompartmentalization of Interface Water Following Protein Association

Normally, association of proteins squeezes patches of bulk-like waters from the interacting surfaces, a process that is energetically favorable [26]. If m represents the average number of soluble oligomers that aggregate into a single molecular cluster, we can obtain an estimate of the recompartmentalization of water in such systems simply by substituting $f^{(A)}/m$ in Eq. 4 for $f^{(A)}$.

As mentioned above, these soluble oligomers will eventually aggregate into larger composites, burying all structural defects inside the newly formed macromolecular assemblies ($f^{(A)} \to f$). Let us assume that all ΔN test isomers are clustered together, forming an aggregate with the water accessible surface area ASA and $f^{(A)} = f$, at equilibrium. Although the total amount of surface water of the newly formed molecular structure may depend on the structural morphology, the thickness (l) of the hydration shell remains in

the same range as for individual peptides, $l \cong 0.11 \dfrac{V_m}{\text{asa}}$. Therefore, we can approximate the amount of water in the surface layer of this molecular composite by $V_s^{(pf)} \cong 0.11 \dfrac{\text{ASA}}{\text{asa}} V_m$. For simplicity, we can consider that $\dfrac{\text{ASA}}{\text{asa}}$ scales with $(\Delta N)^{2/3}$, and hence the volume of water confined at the surface of the composite can be written as $V_s^{(pf)} \cong 0.11\,(\Delta N)^{2/3}\, V_m$. Under such circumstances, the compartmentalization of the interface water can be cast in the form

$$\begin{aligned} X_c^{(pf)} &= \frac{(1-\rho)\,(1-\eta)}{\eta} \\ X_{np}^{(pf)} &= 0.11\, f \frac{1-\eta}{\eta} \frac{N+\Delta N^{2/3}}{N+\Delta N} \\ X_p^{(pf)} &= 0.11\,(1-f)\, \frac{1-\eta}{\eta} \frac{N+\Delta N^{2/3}}{N+\Delta N} \\ X_r^{(pf)} &= 1 - X_c^{(pf)} - X_{np}^{(pf)} - X_p^{(pf)}. \end{aligned} \tag{5}$$

2.5 Water Caged by Protein Aggregation

Long-range interaction between oligomeric composites can also lead to the formation of stable molecular assemblies, caging water molecules inside. The quantity of water sequestered inside the aggregate structure must be in direct proportion with the volume of water bound initially to the surface of individual proteins ($0.11\ \Delta N V_m$) and must depend on the average packing density (ρ_{am}) of the aggregate. Thus, we assume that the volume of caged water within the protein aggregate can be expressed by $V_c^{(am)} \cong 0.11\ \Delta N V_m\,(\rho - \rho_{am})$, where ρ is the packing density of a highly compact aggregation state similar to that of folded proteins (see above). These newly caged water molecules increase the overall amount of buried water $\left(V_c + V_c^{(am)}\right)$ for the entire protein assembly. Therefore, we can write readily

$$\begin{aligned} X_c^{(am)} &= \frac{(\rho_{\max}-\rho)\,(1-\eta)}{\eta} + 0.11 \frac{\Delta N}{N+\Delta N} \frac{1-\eta}{\eta}\,(\rho - \rho_{am}) \\ X_{np}^{(am)} &= 0.11\, f \frac{1-\eta}{\eta} \frac{N+\Delta N^{2/3}}{N+\Delta N} \\ X_p^{(am)} &= 0.11\,(1-f)\, \frac{1-\eta}{\eta} \frac{N+\Delta N^{2/3}}{N+\Delta N} \\ X_r^{(am)} &= 1 - X_c^{(am)} - X_{np}^{(am)} - X_p^{(am)}, \end{aligned} \tag{6}$$

which describes the recompartmentalization of interface water in a system of proteins that forms loose aggregates, caging large amounts of water molecules inside.

3 Results

Morphological changes of the molecular assemblies described above lead to significant modifications of their characteristic hydration profiles. In Fig. 2, we display a histogram

describing the partition of caged water, highly structured surface water, bulk-like water, and remaining water in aqueous environments containing test isomers with increased bulk-like hydrations (see Eq. 4). We compare the hydration profile of a system in which all $N + \Delta N$ constituent proteins have the same value of the parameter $f = f^{(A)} = 0.1$ (control protein background) with the hydration profiles of systems in which the test isomers (ΔN) are characterized by $f^{(A)} > f$, i.e., have more bulk-like water in their hydration shells ($f^{(A)} = 0.3$ and $f^{(A)} = 0.5$). By looking at Fig. 2, we can observe that the amount of surface water with relatively high mobility increases with increasing $f^{(A)}$.

According to Eq. 1, inserting extra amounts of test isomers in the volume V decreases the hydration fraction η. The amount of constrained water molecules increases at the expense of the remaining bulk water, as more water molecules from the bulk water now become surface water. The histogram in Fig. 3 shows the redistribution of water phases following the addition of $\Delta N = 0.2$ mM, $\Delta N = 0.25$ mM, and $\Delta N = 0.3$ mM test isomers.

In Fig. 4a, we display histograms representing the partition of water molecules in the local environment for representative morphological assemblies formed by test isomers. Seemingly, the association of test isomers to form larger composites leads to a progressive elimination of the patches of bulk-like water from protein hydration shells $\left(X_{np} < X_{np}^{(pf)}\right)$. Besides the decrease of the amount of water with bulk-like behavior $\left(X_{np} < X_{np}^{(pf)}\right)$, the association of the test isomers in compact forms leads also to a significant decrease of the highly constrained surface water $\left(X_p < X_p^{(pf)}\right)$, which is caused by the decrease of the water accessible surface area (ASA) of the multimeric composites (Eq. 5). In contrast, during the formation of loose protein aggregates that cage additional water molecules between constituent units $\left(X_c < X_c^{(am)}\right)$, part of the surface water now becomes caged water. This gives rise to a distinct pattern for the compartmentalization of water in the protein system (see Fig. 4).

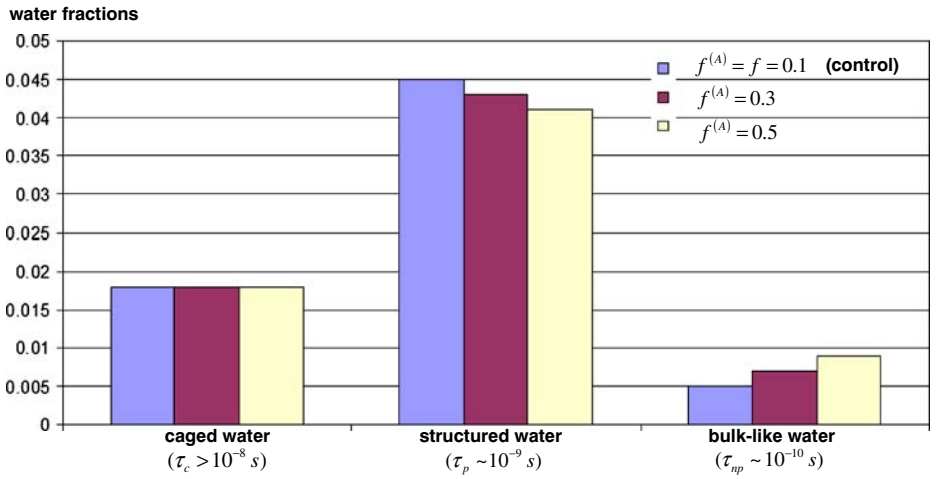

Fig. 2 Histograms describing the partition of constrained water in a system of protein background ($f = 0.1$) plus test isomers with increased surface densities ($f^{(A)} = 0.3$, $f^{(A)} = 0.5$) of patches covered with less structured (bulk-like) water. In computations, we set $V \cong 1\mu m^3$ for the volume of the system and assume $V_m \sim 10^{-9}\mu m^3$ for the molecular volume of a protein

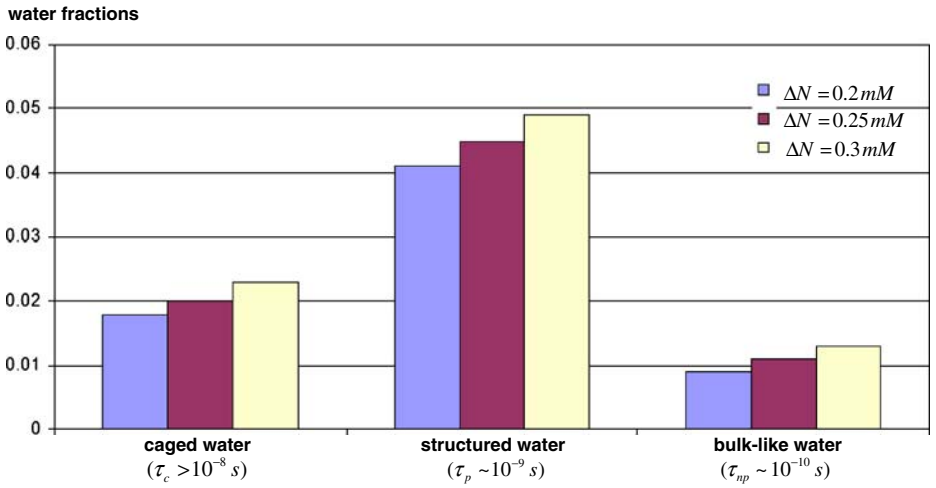

Fig. 3 Distribution of constrained water molecules in the protein system following the addition of various amounts ($\Delta N = 0.2$ mM, $\Delta N = 0.25$ mM, and $\Delta N = 0.3$ mM) of test isomers characterized by surface densities of patches occupied by bulk-like water equal to $f^{(A)} = 0.5$

The present approach provides a mathematical framework for correlating different morphological states of a system of interacting proteins with the characteristic water distribution profiles in the local environment. These hydration profiles $\{X_j\}$ can be used to predict the magnetic relaxation response of surrounding water for each given structural archetype discussed above (i.e., single, soluble oligomers, and aggregates). A physical quantity that describes the magnetic relaxation process is the transverse relaxation time, T_2 [27, 28]. T_2 is a measure of how long the resonant water protons remain coherent or precess in phase following an applied radiofrequency magnetic field. The inverse of the transverse relaxation time reads [27, 28]

$$\frac{1}{T_2} = \sum_j \frac{X_j}{T_{2,j}}, \tag{7}$$

with $1/T_{2,j}$ given by

$$\frac{1}{T_{2,j}} = \frac{C}{2}\left(3\tau_j + \frac{5\tau_j}{1+(\omega_L\tau_j)^2} + \frac{2\tau_j}{1+(2\omega_L\tau_j)^2}\right). \tag{8}$$

Here, ω_L is the Larmor frequency that depends on the intensity of the magnetic field (B_0) and proton gyromagnetic ratio ($\gamma = 2.67510^8$ $s^{-1}T^{-1}$), $\omega_L = \gamma B_0$ and C is a constant measuring the strength of the magnetic dipolar interaction, $C = 1.0210^{10}$ s^{-2} for water protons. τ_j represents the relaxation time of the water molecules in each water phase X_j, $\tau_j \in \{\tau_c, \tau_p, \tau_{np}, \tau_r\}$. Both experiments [4, 19, 20, 29, 30] and theory [1, 5, 7, 9, 24] suggest the following hierarchy $\tau_r < \tau_{np} < \tau_p < \tau_c$, where $\tau_r \cong 10^{-12}$ s characterizes the mobility of water with no constraints [7, 9]; $\tau_{np} \cong 10^{-10}$ s represents the average relaxation time of bulk-like water on the protein surface [4, 9, 19, 20, 29, 30]; $\tau_p \cong 10^{-9}$ is the typical relaxation time of highly structured surface water [4, 9, 19, 20] and $\tau_c > 10^{-8}$ s stands for the relaxation time of immobile water molecules buried in macromolecular structures [1, 9, 29, 30].

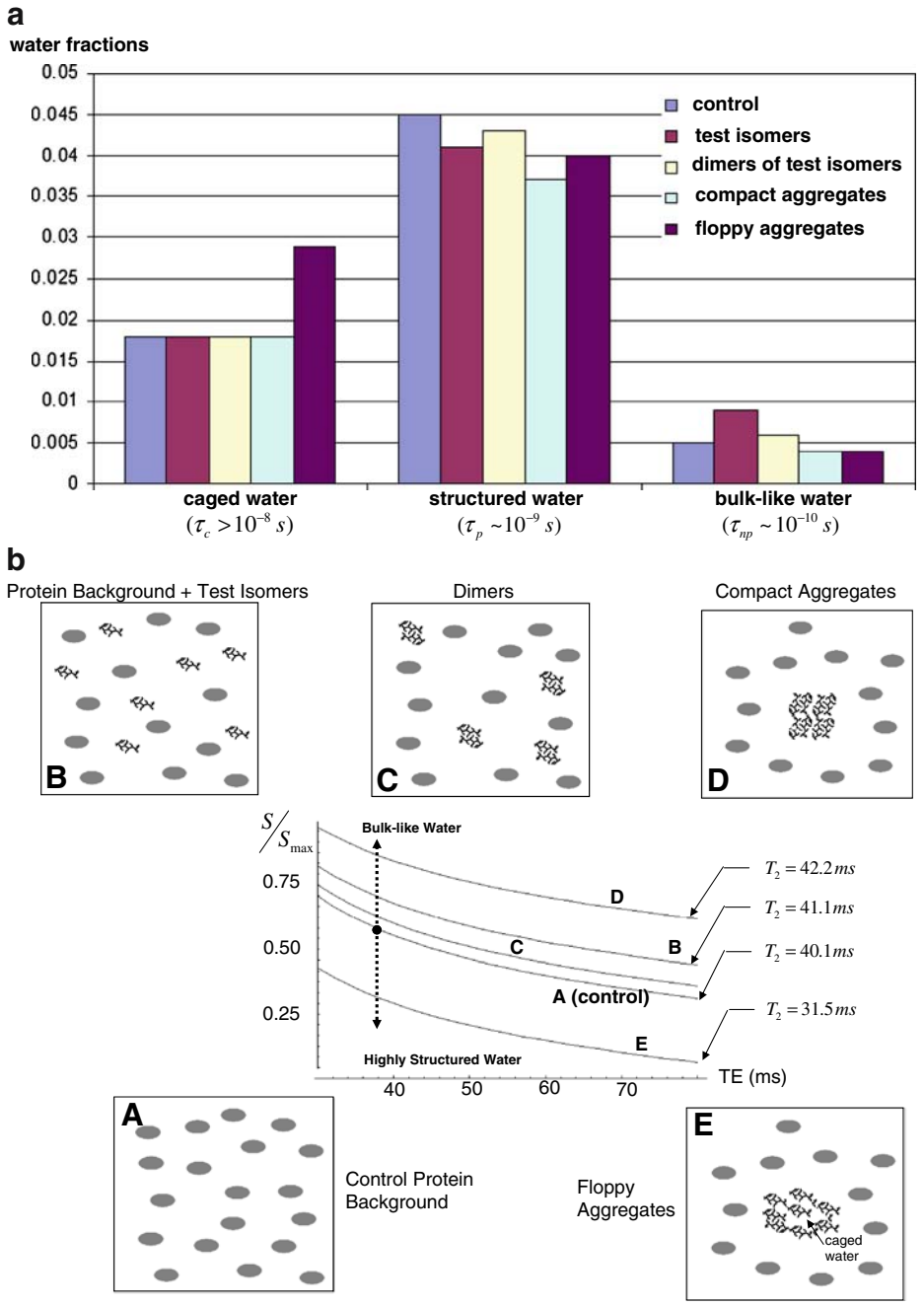

Fig. 4 **a** Histograms describing the redistribution of hydration water over the characteristic clusters of relaxation times for representative morphological assemblies formed by test isomers in the local environment. In computations, we set $V \cong 1\mu m^3$ for the volume of the system and assume $V_m \sim 10^{-9}\mu m^3$ for the molecular volume of a protein. **b** The predicted change of the pixel intensity of the MR image (S/S_{max}) as a function of the echo times (TE) and the characteristic magnetic relaxation times (T_2) corresponding to distributions of constrained water displayed in Fig. 4a

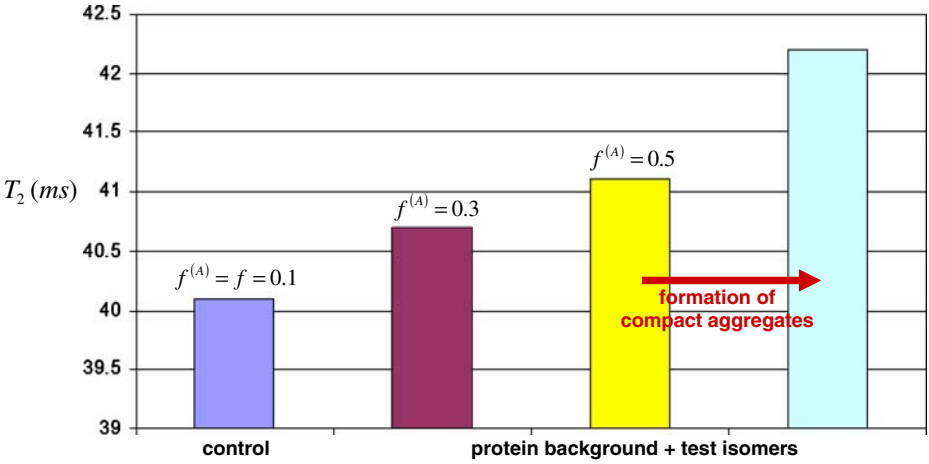

Fig. 5 The increase of the fraction of surface water molecules with a bulk-like behavior leads to an increase of the T_2 relaxation time. The *last bar* shows the change of the T_2 value following the association of test isomers ($f^{(A)} = 0.5$) in compact aggregates that are characterized by hydration profiles of the type given in Eq. 5

From Eq. 7, we can infer that the difference between various partitions of the water phases in the volume V following the addition of the test isomers is the source of the magnetic resonance contrast between morphological states of the protein system. To predict the T_2 values corresponding to typical hydration profiles discussed above, and shown in Fig 4b, we use Eq. 8 with X_j given by Eqs. 4–6. In computations, we set $B_0 = 9.4T$ for the applied magnetic field. The first three bars in Fig. 5 show the effective T_2 values corresponding to hydration profiles of test isomers that are characterized by $f^{(A)} > f$, i.e., have more bulk-like water in their hydration shells ($f^{(A)} = 0.3$ and $f^{(A)} = 0.5$). Not surprisingly, large values of the fraction of surface water molecules with a bulk-like behavior (see Fig. 2) lead to an increase of the magnetic relaxation time, i.e., from $T_2 = 40.1$ ms in control to $T_2 = 40.7$ ms and $T_2 = 41.1$ ms for the test isomers. The last bar in Fig. 5 shows the change of the T_2 value following the association of test isomers ($f^{(A)} = 0.5$) in compact aggregates that are characterized by hydration profiles of the type given in Eq. 5. Based in the results displayed in Fig. 5, one can expect that the overall magnetic relaxation signal of water in such environments to be shifted towards values that correspond to the magnetic signal of bulk water. Such a shift may indicate that the addition of test isomers having large values of their characteristic parameter $f^{(A)}$ ($f^{(A)} > f$) gives rise to MR imaging (MRI) domains (voxels) that appear brighter on T_2-weighted MR images than similar volumes in which the $N + \Delta N$ proteins have $f^{(A)} = f$ (control protein background).

4 Discussion

Within the present work, we investigated the partition of constrained water molecules following the addition to the existing protein background of various test isomers bearing surface patches occupied by highly mobile water molecules. We derived simple

mathematical equations correlating the characteristic water populations X_j (bulk, caged, and the two categories of surface hydration water, i.e., structured and bulk-like) with structural parameters of the system, such as hydration fraction (η), protein numbers (N, ΔN), relative packing density ($\rho_{max} - \rho$), and fractions of surface patches of bulk-like waters (f, $f^{(A)}$). We also analyzed the change of the water partition after the association of the test isomers in distinct aggregation states, i.e., small compact composites that are formed by expelling water between constituent units and loose aggregates that cage water inside the structure. Our study shows that distinct morphological states of these protein systems are characterized by well-defined fractions of confined water at specific locations of the molecular structures.

Our results suggest that microscopic environments containing protein isomers that have lower energies of interaction with surrounding water (i.e., increased surface densities of patches occupied by water with a bulk-like behavior) as well as small soluble composites and compact aggregates formed by these isomers are likely to give rise to hyperintense magnetic contrasts (increased T_2 values). On a grayscale, the pixel intensities of the MR images of such environments (voxels) will appear brighter than the control protein background (see the middle bars in Fig. 5), with the magnetic contrast corresponding to a compact aggregate being the brightest (see the last bar in Fig. 5).

It is worthwhile to note at this point several recent studies on the polymerization of amyloid beta units into fibers. Although initial studies of the amyloid structures suggested that the strands composing the fibrils are filled with water [31, 32], recent data indicate that this is unlikely [33–35]. Studies probing the stability of amyloid fibers suggest that water exclusion is part of the temporal transition transition process from the early stage of amorphous aggregation to that of fibrillation [36]. During the maturation phase, side chain packing and intramolecular hydrogen bond formation between beta-sheets are optimized [36]. Therefore, the packing of amyloid peptides in fibril strands reaches the optimum value while, water in the interior of the fibril strands vanishes. Indeed, X-ray diffraction studies revealed the existence of a completely dry interface between beta-strands from which it was concluded that the stable structural unit of the cross-beta spine is a pair of beta-sheets [34]. Interestingly, the study shows that, in contrast with the interface between the two tightly bonded beta-sheets in a pair which is dry, the separation between two adjacent structural units in microcrystals is lined with water molecules, forming a wet interface [34]. Therefore, we cannot rule out the possibility that mature amyloid plaques, formed by the accumulation of large amyloid fibrils in the extracellular environment, contain water molecules caged between the constituent fibrils. In light of experimental observations [33–35] and based on the present theoretical results, we suggest that nascent amyloid protofibrils can be detected based on the magnetic contrast produced by the water constrained at interfaces. Soluble amyloid oligomers and nascent fibrils have less structured water and virtually lack caged water. They will induce hyperintense signals in the characteristic voxels as well as increased T_2 relaxation times. This will be in contrast with large plaques constituted by the association of many fibrils which are identified as dark spots on gray normal background tissue [37–41].

Our study may prove useful in generating new testable predictions of circumstances related to the presence of amyloidogenic proteins in a given aqueous environment. Progress in understanding the chemistry effects induced by such molecular entities on the dynamics of the surrounding water in combination with data from new MR spectroscopic methods for determining the overexpression of abnormal proteins and their state of association in the cell [42, 43] can help in designing efficient MRI protocols to be used in detecting the early molecular alterations in amyloidogenic diseases.

Refinements of the present theory can be obtained by using molecular dynamics (MD) simulations and MRI measurements of protein solutions. MD simulations of the oligomerization process of amyloidogenic proteins are becoming increasingly relevant [44–47]. However, an explicit atomistic description of the solvation phenomena described in the present work remains computationally very expensive, due to the very large number of participating water molecules. In principle, the access of the MD simulations to the conformational space and time scales of interest here can be facilitated by describing water-mediated interactions between amyloidogenic units by a potential function of the type we proposed recently [48]. The use of potential functions of this type has been shown to lead to a marked improvement in protein structure prediction [49].

Acknowledgements F.D. acknowledges that part of this work was done at the John von Neumann Institute for Computing, Research Center Jülich, Germany. The research of A.F. is supported by NIH grant R01-GM072614. L.R.S. would like to acknowledge support from the Institute for Biophysical Dynamics at the University of Chicago.

References

1. Makarov, V.A., Andrews, B.K., Smith, P.E., Pettitt, B.M.: Residence times of water molecules in the hydration sites of myoglobin. Biophys. J. **79**, 2966–2974 (2000)
2. Fenimore, P.W., Frauenfelder, H., McMahon, B.H., Parak, F.G.: Slaving: solvent fluctuations dominate protein dynamics and functions. Proc. Natl. Acad. Sci. U. S. A. **99**, 16047–16051 (2002). doi:10.1073/pnas.212637899
3. Pal, S.K., Peon, J., Zewail, A.H.: Biological water at the protein surface: dynamical solvation probed directly with femtosecond resolution. Proc. Natl. Acad. Sci. U. S. A. **99**, 1763–1768 (2002). doi:10.1073/pnas.042697899
4. Bhattacharyya, S.M., Wang, Z.-G., Zewail, A.H.: Dynamics of water near a protein surface. J. Phys. Chem. B **107**, 13218–13228 (2003). doi:10.1021/jp030943t
5. Despa, F., Fernández, A., Berry, R.S.: Dielectric modulation of biological water. Phys. Rev. Lett. **93**, 228104 (2004). doi:10.1103/PhysRevLett.93.228104
6. Modig, K., Liepinsh, E., Otting, G., Halle, B.: Dynamics of protein and peptide hydration. J. Am. Chem. Soc. **126**, 102–114 (2004). doi:10.1021/ja038325d
7. Russo, D., Murarka, R.K., Copley, J.R., Head-Gordon, T.: Molecular view of water dynamics near model peptides. J. Phys. Chem. B **109**, 12966–12975 (2005). doi:10.1021/jp051137k
8. Despa, F.: Biological water, its vital role in macromolecular structure and function. Ann. N. Y. Acad. Sci. **1066**, 1–11 (2005). doi:10.1196/annals.1363.023
9. De Simone, A., Dodson, G.G., Verma, C.S., Zagari, A., Fraternali, F.: Prion and water: tight and dynamical hydration sites have a key role in structural stability. Proc. Natl. Acad. Sci. U. S. A. **102**, 7535–7540 (2005). doi:10.1073/pnas.0501748102
10. Li, T., Hassanali, A.A., Kao, Y.T., Zhong, D., Singer, S.J.: Hydration dynamics and time scales of coupled water-proton fluctuations. J. Am. Chem. Soc. **129**, 3376–3382 (2007). doi:10.1021/ja0685957
11. Despa, F., Berry, R.S.: The origin of long range attraction between hydrophobes in water. Biophys. J. **92**, 373–378 (2007). doi:10.1529/biophysj.106.087023
12. De Simone, A., Zagari, A., Derreumaux, P.: Structural and hydration properties of the partially unfolded states of the prion protein. Biophys. J. **93**, 1284–1292 (2007). doi:10.1529/biophysj.107.108613
13. Frauenfelder, H., Fenimore, P.W., Young, R.D.: Protein dynamics and function: insights from the energy landscape and solvent slaving. IUBMB Life **16**, 669–678 (2007)
14. Ball, P.: Water as an active constituent in cell biology. Chem. Rev. **108**, 74–108 (2008). doi:10.1021/cr068037a
15. Fernández, A., Berry, R.S.: Extent of hydrogen-bond protection in folded proteins: a constraint on packing architectures. Biophys. J. **83**, 2475–2481 (2002)
16. Fernández, A., Berry, R.S.: Molecular dimension explored in evolution to promote proteomic complexity. Proc. Natl. Acad. Sci. U. S. A. **101**(101), 13460–13465 (2004). doi:10.1073/pnas.0405585101

17. Fernández, A., Scott, R., Berry, R.S.: The nonconserved wrapping of conserved protein folds reveals a trend towards increasing connectivity in proteomic networks. Proc. Natl. Acad. Sci. U. S. A. **101**, 2823–2827 (2004). doi:10.1073/pnas.0308295100
18. Fernández, A., Scott, R., Berry, R.S.: Packing defects as selective switches for drug-based protein inhibitors. Proc. Natl. Acad. Sci. U. S. A. **103**(2), 323–328 (2006)
19. Denisov, V.P., Halle, B.: Thermal denaturation of ribonuclease A characterized by water 17O and 2H magnetic relaxation dispersion. Biochemistry **37**, 9595–9604 (1998). doi:10.1021/bi980442b
20. Denisov, V.P., Halle, B.: Hydration of denatured and molten globule proteins. Nat. Struct. Biol. **6**, 253–260 (1999). doi:10.1038/6692
21. Chalikian, T.V., Totrov, M., Abagyan, R., Breslauer, K.J.: The hydration of globular proteins as derived from volume and compressibility measurements: cross correlating thermodynamic and structural data. J. Mol. Biol. **260**, 588–603 (1996). doi:10.1006/jmbi.1996.0423
22. Jaeger, H.M., Nagel, S.R.: Physics of the granular state. Science **255**, 1523–1531 (1992). doi:10.1126/science.255.5051.1523
23. Makhatadze, G., Privalov, P.A.: Energetics of protein structure. Adv. Protein Chem. **47**, 307–425 (1995). doi:10.1016/S0065-3233(08)60548-3
24. Petukhov, M., Rychkov, G., Firsov, L., Serrano, L.: H-bonding in protein hydration revisited. Protein Sci. **13**, 2120–2129 (2004). doi:10.1110/ps.04748404
25. Reiss, H.: Scaled particle methods in the statistical thermodynamics of fluids. Adv. Chem. Phys. **9**, 1–84 (1965). doi:10.1002/9780470143551.ch1
26. Fernández, A.: What factor drives the fibrillogenic association of beta-sheets. FEBS Lett. **579**, 6635–6640 (2005). doi:10.1016/j.febslet.2005.10.058
27. Zimmerman, J.R., Brittin, W.E.: Nuclear magnetic resonance studies in multiple phase systems: lifetime of a water molecule in an absorbing phase on silica gel. J. Phys. Chem. **6**, 1328–1333 (1957). doi:10.1021/j150556a015
28. Bryant, R.G.: The dynamics of water–protein interactions. Annu. Rev. Biophys. Biomol. Struct. **25**, 29–53 (1996). doi:10.1146/annurev.bb.25.060196.000333
29. Denisov, V.P., Peters, J., Horlein, H.D., Halle, B.: Using buried water molecules to explore the energy landscape of proteins. Nat. Struct. Biol. **3**, 505–509 (1996). doi:10.1038/nsb0696-505
30. Foster, K.R., Resing, H.A., Garroway, A.N.: Bounds on "bound water": transverse nuclear magnetic resonance relaxation in barnacle muscle. Science **194**, 324–326 (1976). doi:10.1126/science.968484
31. Perutz, M.F., Finch, J.T., Berriman, J., Lesk, A.: Amyloid fibers are water-filled nanotubes. Proc. Natl. Acad. Sci. U. S. A. **99**, 5591–5595 (2002). doi:10.1073/pnas.042681399
32. Kishimoto, A., Hasegawa, K., Suzuki, H., Taguchi, H., Namba, K., Yoshida, M.: β-Helix is a likely core structure of yeast prion Sup35 amyloid fibers. Biochem. Biophys. Res. Commun. **315**, 739–745 (2004). doi:10.1016/j.bbrc.2004.01.117
33. Petkova, A.T., Leapman, R.D., Guo, Z.H., Yau, W.M., Mattson, M.P., Tycko, R.: Self-propagating, molecular-level polymorphism in Alzheimer's β-amyloid fibrils. Science **307**, 262–265 (2005). doi:10.1126/science.1105850
34. Nelson, R., Sawaya, M.R., Balbirnie, M., Madsen, A.Ø., Riekel, C., Grothe, R., Eisenberg, D.: Structure of the cross-β spine of amyloid-like fibrils. Nature **435**, 773–778 (2005). doi:10.1038/nature03680
35. Paravastu, A.K., Petkova, A.T., Tycko, R.: Polymorphic fibril formation by residues 10–40 of the Alzheimer's beta-amyloid peptide. Biophys. J. **90**, 4618–4629 (2006). doi:10.1529/biophysj.105.076927
36. Meersman, F., Dobson, C.M.: Probing the pressure–temperature stability of amyloid fibrils provides new insights into their molecular properties. Biochim. Biophys. Acta **1764**, 452–460 (2006)
37. Benveniste, H., Einstein, G., Kim, K.R., Hulette, C., Johnson, G.A.: Detection of neuritic plaques in Alzheimer's disease by magnetic resonance microscopy. Proc. Natl. Acad. Sci. U. S. A. **96**, 14079–14084 (1999). doi:10.1073/pnas.96.24.14079
38. Lee, S.P., Falangola, M.F., Nixon, R.A., Duff, K., Helpern, J.A.: Visualization of beta-amyloid plaques in a transgenic mouse model of Alzheimer's disease using MR microscopy without contrast reagents. Magn. Reson. Med. **52**, 538–544 (2004). doi:10.1002/mrm.20196
39. Jack, C.R. Jr., Garwood, M., Wengenack, T.M., Borowski, B., Curran, G.L., Lin, J., Adriany, G., Grohn, O.H., Grimm, R., Poduslo, J.F.: In vivo visualization of Alzheimer's amyloid plaques by magnetic resonance imaging in transgenic mice without a contrast agent. Magn. Reson. Med. **52**, 1263–1271 (2004). doi:10.1002/mrm.20266
40. Jack, C.R. Jr., Wengenack, T.M., Reyes, D.A., Garwood, M., Curran, G.L., Borowski, B.J., Lin, J., Preboske, G.M., Holasek, S.S., Adriany, G., Poduslo, J.F.: In vivo magnetic resonance microimaging

of individual amyloid plaques in Alzheimer's transgenic mice. J. Neurosci. **25**, 10041–10048 (2005). doi:10.1523/JNEUROSCI.2588-05.2005
41. Vanhoutte, G., Dewachter, I., Borghgraef, P., Van Leuven, F., Van der Linden, A.: Noninvasive in vivo MRI detection of neuritic plaques associated with iron in APP[V717I] transgenic mice, a model for Alzheimer's disease. Magn. Reson. Med. **53**, 607–613 (2005). doi:10.1002/mrm.20385
42. Selenko, P., Serber, Z., Gadea, B., Ruderman, J., Wagner, G.: Quantitative NMR analysis of the protein G B1 domain in Xenopus laevis egg extract and intact oocytes. Proc. Natl. Acad. Sci. U. S. A. **103**, 11904–11909 (2006). doi:10.1073/pnas.0604667103
43. Charlton, L.M., Pielak, G.J.: Peeking into living eukaryotic cells with high-resolution NMR. Proc. Natl. Acad. Sci. U. S. A. **103**, 11817–11818 (2006). doi:10.1073/pnas.0605297103
44. Urbanc, B., Cruz, L., Yun, S., Buldyrev, S.V., Bitan, G., Teplow, D.B., Stanley, H.E.: In silico study of amyloid β-protein folding and oligomerization. Proc. Natl. Acad. Sci. U. S. A. **101**, 17345–17350 (2004). doi:10.1073/pnas.0408153101
45. Buchete, N.-V., Tycko, R., Hummer, G.: Molecular dynamics simulations of Alzheimer's β-amyloid protofilaments. J. Mol. Biol. **353**, 804–821 (2005)
46. Cox, D.L., Sing, R.R.P., Yang, S.: Prion disease: exponential growth requires membrane binding. Biophys. J. **90**, L77–L79 (2006). doi:10.1529/biophysj.106.081703
47. Zheng, J., Jang, H., Ma, B., Nussinov, R.: Annular structures as intermediates in fibril formation of Alzheimer Aβ_{17-42}. J. Phys. Chem. B **112**, 6856–6865 (2008). doi:10.1021/jp711335b
48. Despa, F., Berry, R.S.: Hydrophobe–water interactions: methane as a model. Biophys. J. **95**, 4241–4245 (2008)
49. Lin, M.S., Fawzi, N.L., Head-Gordon, T.: Hydrophobic potential of mean force as a solvation function for protein structure prediction. Structure **15**, 727–740 (2007). doi:10.1016/j.str.2007